Order Versus Disorder in Chiral Tetrathiafulvalene-Oxazoline Radical-Cation Salts: Structural and Theoretical Investigations and Physical Properties

Augustin M. Madalan,[a] Céline Réthoré,[a] Marc Fourmigué,[b] Enric Canadell,[c] Elsa B. Lopes,[d] Manuel Almeida,[d] Pascale Auban-Senzier,[e] and Narcis Avarvari*[a]

Abstract: Electrocrystallization experiments with the chiral ethylenedithio-tetrathiafulvalene-methyl-oxazoline (EDT-TTF-OX) donors (R)-, (S)-, and (rac)-**1** have provided two series of mixed-valence salts with the PF_6^- and $[Au(CN)_2]^-$ anions. Within each series the cell parameters are the same for the three R, S, and rac compounds, except for the space group, which is centrosymmetric triclinic $P\bar{1}$ for the racemic forms and noncentrosymmetric $P1$ for the enantiopure salts. In the racemic salt $[(rac)$-**1**$]_2PF_6$ the two enantiomers crystallize disordered on the same crystallographic site with a site occupational factor of 0.6:0.4, whereas this type of disorder is not possible in the enantiopure salts. Both s-cis and s-trans conformations, when taking into account the mutual orientation of the TTF and oxazoline moieties, are present in this first series. In sharp contrast, in the series of salts $[1]_2[Au(CN)_2]$, only the s-trans conformation is observed with no structural disorder. Theoretical calculations at the DFT level of theory revealed a very small energy difference between the two stable planar s-cis and s-trans conformations, which are both energy minima in either neutral or oxidized states. Single-crystal conductivity measurements showed metallic-like behavior for all the salts down to 220–250 K with a smooth increase in resistivity at lower temperatures. The conductivity at room temperature is $5\,\mathrm{S\,cm^{-1}}$ for $[(rac)$-**1**$]_2PF_6$, in which disorder was observed, whereas for $[(R)$-**1**$]_2PF_6$ and $[(S)$-**1**$]_2PF_6$ the average value is around $100\,\mathrm{S\,cm^{-1}}$. In the second series of salts the conductivity at room temperature is 125–$130\,\mathrm{S\,cm^{-1}}$ for $[(rac)$-**1**$]_2[Au(CN)_2]$ and $[(R)$-**1**$]_2[Au(CN)_2]$. Extended Hückel band structure calculations revealed identical features for the three salts of the $[1]_2[Au(CN)_2]$ series and are consistent with the electronic structures of quasi-one-dimensional conductors.

Keywords: chirality · conducting materials · density functional calculations · mixed-valent compounds · X-ray diffraction

Dedicated to Professor Michel Geoffroy on the occasion of his 65th birthday and retirement

[a] Dr. A. M. Madalan, Dr. C. Réthoré, Dr. N. Avarvari
Université d'Angers, CNRS
Laboratoire de Chimie et Ingénierie Moléculaire
CIMA UMR 6200, UFR Sciences, Bât. K, 2 Bd. Lavoisier
49045 Angers (France)
Fax: (+33) 0241-73-54-05
E-mail: narcis.avarvari@univ-angers.fr

[b] Dr. M. Fourmigué
Sciences Chimiques de Rennes
UMR 6226 CNRS-Université Rennes I
Campus de Beaulieu, 35042 Rennes (France)

[c] Dr. E. Canadell
Institut de Ciència de Materials de Barcelona (CSIC)
Campus de la UAB
08193 Bellaterra (Spain)

[d] Dr. E. B. Lopes, Dr. M. Almeida
Dept. Química, ITN/CFMCUL, 2686-953 Sacavém (Portugal)

[e] Dr. P. Auban-Senzier
Laboratoire de Physique des Solides, UMR 8502
Bât. 510, Université Paris-Sud
91405 Orsay (France)

Supporting information for this article is available on the WWW under http://dx.doi.org/10.1002/chem.200901980. Geometries, equilibrium energies with zero-point corrections, low frequencies, and cartesian coordinates for the optimized structures of s-trans **1′**, s-cis **1′**, ˙s-trans **1′+**, and ˙s-cis **1′+**. Single-crystal X-ray data and additional structural figures, conductivity measurements, and band structure calculations are provided.

Introduction

The synthesis of functional molecular conductors with at least one physical property in addition to electronic conductivity is a very active area of research in the more general field of multifunctional molecular materials.[1] In this respect, the introduction of chiral information into electroactive precursors and the corresponding molecular conductors is particularly interesting for several reasons.[2] One of the main ones is the possibility of detecting the electrical magneto-chiral anisotropy effect, which expresses the synergy between chirality and conductivity in the transport properties of a conductor in a magnetic field parallel to the direction of the current.[3] Experimental evidence for this relatively new phenomenon is still very scarce, and has been provided, for example, by Rikken and co-workers in the case of chiral carbon nanotubes.[4] However, other interesting applications such as chiroptical conductors,[5] chiroptical redox switches,[6] electroactive helical architectures through supramolecular chirality[7] have emerged within the last few years. Because the large majority of molecular conductors and superconductors are based on tetrathiafulvalene (TTF) derivatives,[8] a most useful family of organic redox-active molecules,[9] much effort is currently being directed towards the synthesis of enantiopure TTFs[2] with the ultimate goal to produce chiral-conducting materials. Accordingly, several families of chiral TTFs, for example, bis(ethylenedithio)-tetrathiafulvalene (BEDT-TTF) derivatives,[10] EDT-TTF-oxazolines (EDT = ethylenedithio),[11] EDT-TTF-bis(oxazolines),[12] TTFs with chiral side chains,[13] bis(pyrrolo)-TTFs,[14] and TTF-sulfoxides[15] have been described (Figure 1).
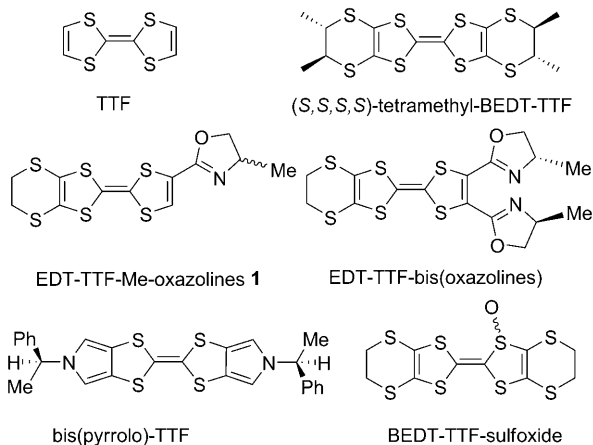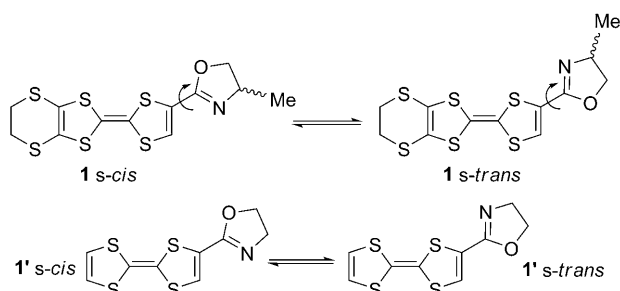

Figure 1. Examples of chiral TTFs.

Note that Dunitz and co-workers described in the middle of the eighties the first enantiopure TTF donor, (S,S,S,S)-tetramethyl-BEDT-TTF.[16] However, in spite of the large number of chiral enantiopure precursors available to date, only a relatively small number of conducting chiral salts have been prepared. For example, the donor (S,S,S,S)-tetra-

methyl-BEDT-TTF provided a series of 2:1 semiconducting salts with octahedral anions (PF_6^-, AsF_6^-, and SbF_6^-), whereas metallic-like behavior was observed in salts with tetrahedral anions (BF_4^- and ClO_4^-) and $\approx$3:2 stoichiometry.[17] Note also the remarkable 2:1 κ phase obtained from the donor (S,S)-dimethyl-BEDT-TTF with the ClO_4^- anion, for which a likely superconducting state was observed below 2 K under 5 kbar pressure.[18] In all these examples either one or other enantiomer, and sometimes the racemic form, were described, but never the complete series, that is, the two enantiomers as well as the racemate. However, with (rac)-, (R)-, and (S)-EDT-TTF-methyl-oxazolines (Figure 1),[11] we recently reported the first example of a complete series of 2:1 conducting salts with the octahedral AsF_6^- anion.[19] Most remarkably, the enantiopure salts proved to be about one order of magnitude more conducting at room temperature than the racemic one, with metallic-like behavior for the three of them in a high-temperature regime, despite identical structural features and band dispersions. This difference in conductivity is very likely due to the structural disorder present in the racemic salt, in which both enantiomers crystallized statistically in a 1:1 ratio on the same crystallographic site, whereas disorder was absent in the enantiopure salts. Knowing that the structural disorder can strongly influence the electronic conductivity,[20] these results highlighted the role of chirality in the modulation of the structural disorder in the solid state, and thus its influence on conductivity. Note that a closely related effect was evidenced by Martin et al. in the conducting mixed-valence salts of $[BEDT-TTF]_4[(NH_4)Fe(ox)_3]$ (ox = oxalate) containing one molecule of either racemic or (S)-sec-phenethyl alcohol.[21] A more pronounced metal-to-insulator transition was observed in the former, in which the racemic molecules of the solvent exhibited an occupational disorder that was absent in the latter. As a continuation of our efforts, we describe in this report two new complete series of chiral radical-cation salts based on the series EDT-TTF-methyl-oxazolines (EDT-TTF-OX, **1**), in which the order/disorder balance, modulated both by the chiral information and the anion, plays an important role in the conducting properties of these molecular materials.
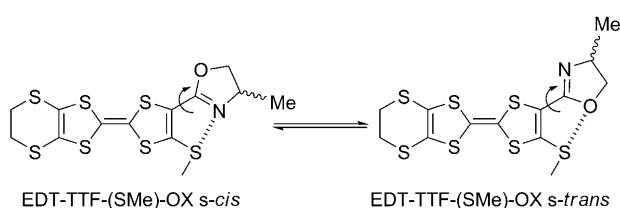
Results and Discussion

Stable conformations of EDT-TTF-OX (1): The chiral donors we have used as precursors for the radical-cation salts are the (rac)-, (R)-, and (S)-EDT-TTF-methyl-oxazolines (**1**), synthesized according to the published procedure.[11] These donors are likely to exist in two stable planar conformations, that is, s-cis and s-trans (Scheme 1), when considering the relative orientation of the oxazoline ring with respect to the TTF and the possibility of free rotation around the C—C bond connecting the two fragments.

In previous work we investigated a series of EDT-TTF-(SMe)-oxazolines containing a methylthio substituent on TTF ortho to the oxazoline ring with the primary aim to

Scheme 1. Conformations of EDT-TTF-Me-OX (**1**) and the model analogues **1′**.

Figure 2. Equilibrium geometries for s-*trans* **1′** (top) and s-*cis* **1′** (bottom).

favor 1,5-nonbonded S···N or S···O interactions (Scheme 2).[22]

Scheme 2. Stable conformations of EDT-TTF-SMe-OX.

The corresponding theoretical study of the model donor TTF-(SMe)-OX (in which the ethylenedithio bridge was discarded) showed that both s-*cis* and s-*trans* conformations were energy minima with a very small energy difference between them. Experimentally, only the s-*trans* conformation of the neutral donor EDT-TTF-(SMe)-OX was observed in the solid state, whereas in the series of radical-cation salts the s-*trans* and s-*cis* conformations coexisted. This was in agreement with the theoretical calculations, which showed that, upon oxidation, the s-*cis* conformation is energetically slightly more favorable than the s-*trans* conformation when compared with the neutral precursors.

Analogously, the donors **1**, and also the homologues containing an isopropyl substituent instead of a methyl group, crystallize only as s-*trans* conformers,[11] whereas in the series of radical-cation salts [**1**]₂AsF₆, both conformations were present in the crystal structures. Therefore, to estimate the relative stability of the two planar conformations in the neutral and radical-cation states of the donors **1**, we performed theoretical calculations on the model TTF-oxazoline **1′** (Scheme 1). Geometry optimizations together with harmonic frequency calculations were performed at the DFT level with the B3LYP functional and 6-31+G* basis set. As anticipated, two energy minima were obtained for the neutral **1′** corresponding to the s-*trans* and s-*cis* conformations (Figure 2). The dihedral angle TTF···oxazoline in both cases is practically 0°, in agreement with the experimental structure of s-*trans* **1**,[11] for which a value of 4.5° was determined. The energy difference $\Delta E = E_{s\text{-}cis} - E_{s\text{-}trans}$ between the two
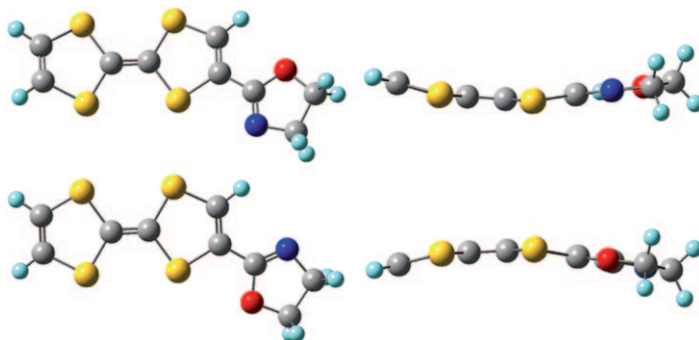
optimized geometries amounts to only 1.41 kcal mol^{-1}, which indicates that the s-*trans* conformation is slightly more stable in the gas phase than s-*cis*, in accord with the fact that only the s-*trans* conformation was observed in the solid-state structure of **1**.

For both conformations the HOMO is of the classic TTF π type, whereas the LUMO, also of π type, is mainly delocalized over the oxazoline ring and the adjacent dithiol half of the TTF (see the Supporting Information). Unrestricted geometry optimization of the radical cation of **1′** at the same level of theory also resulted in two energy minima corresponding to the planar s-*trans* and s-*cis* conformations (see the Supporting Information), in good agreement with the experimental solid-state structure of [**1**]$^{+}$[19] for which both conformations were observed. Note that now the energy difference $\Delta E = E_{s\text{-}cis} - E_{s\text{-}trans}$ between the optimized conformations is 1.38 kcal mol^{-1}, that is, slightly smaller than for the neutral precursors. However, it is clear that both conformations are likely to exist in the solid state, and only packing effects or additional intermolecular interactions, not taken into account in the calculations, are responsible for the experimental observation of either one or both of them. One of the parameters that can play a subtle role in the packing of the oxidized donors in the solid state is the anion provided by the supporting electrolyte used in the electrocrystallization experiment. As outlined before, the previous series of conducting mixed-valence salts contained the octahedral monoanion hexafluoroarsenate AsF₆$^{-}$. To introduce only a small variation in the size or shape, we used in this study the smaller octahedral anion hexafluorophosphate PF₆$^{-}$ and the linear anion gold dicyanide [Au(CN)₂]$^{-}$.

Two complete series of mixed-valence salts of EDT-TTF-OX (1): Electrocrystallization of the series of (*rac*)-, (*R*)- and (*S*)-**1** in the presence of [(*n*Bu)₄N]PF₆ as supporting electrolyte and acetonitrile as solvent afforded black crystalline needles on the anode that were of suitable quality for single-crystal X-ray structure determination. The three mixed-valence salts are formulated as [**1**]₂PF₆ and are isostructural with their corresponding AsF₆$^{-}$ counterparts.[19] Indeed, the cell parameters are basically the same and the space groups are triclinic $P\bar{1}$ for the racemic salt and $P1$ for

the enantiopure salts (Table 1). In the racemic salt there is one independent donor molecule in a general position in the asymmetric unit and the anion lies on the inversion center. Thus, the unit cell contains two donor molecules and one anion. The absence of the inversion center in the crystal structures of the enantiopure salts implies the existence of

Table 1. Crystallographic data, details of data collection and structure refinement parameters for $PF_6^{<M\cdot>}$ and $Au(CN)_2^-$ salts of **1**.

Compound	[(rac)-**1**]$_2$PF$_6$	[(R)-**1**]$_2$PF$_6$	[(S)-**1**]$_2$PF$_6$
formula	C$_{24}$H$_{22}$F$_6$N$_2$O$_2$PS$_{12}$	C$_{24}$H$_{22}$F$_6$N$_2$O$_2$PS$_{12}$	C$_{24}$H$_{22}$F$_6$N$_2$O$_2$PS$_{12}$
M [g mol^{-1}]	900.13	900.13	900.13
T [K]	293(2)	293(2)	293(2)
crystal system	triclinic	triclinic	triclinic
space group	$P\bar{1}$	$P1$	$P1$
a [Å]	6.4048(9)	6.3924(5)	6.3810(7)
b [Å]	7.4975(12)	7.4989(6)	7.4739(8)
c [Å]	17.847(3)	17.8464(10)	17.796(2)
α [°]	83.477(19)	83.061(5)	83.073(13)
β [°]	86.272(18)	86.311(6)	86.460(13)
γ [°]	85.434(18)	85.558(6)	85.547(13)
V [Å^3]	847.4(2)	845.36(12)	838.79(16)
Z	2	2	2
ρ_{calcd} [g cm^{-3}]	1.764	1.776	1.782
μ [mm^{-1}]	0.885	0.891	0.894
$F(000)$	457	457	457
GOF on F^2	0.848	1.016	0.808
final $R1$, wR^2 [$I > 2\sigma(I)$]	0.0380, 0.0764	0.0385, 0.0802	0.0339, 0.0612
$R1$, wR_2 (all data)	0.0796, 0.0856	0.0673, 0.0887	0.0858, 0.0711
largest diff. peak and hole [e Å^{-3}]	0.482, −0.463	0.533, −0.303	0.370, −0.299
compound	[(rac)-**1**]$_2$[Au(CN)$_2$]	[(R)-**1**]$_2$[Au(CN)$_2$]	[(S)-**1**]$_2$[Au(CN)$_2$]
formula	C$_{26}$H$_{22}$AuN$_4$O$_2$S$_{12}$	C$_{26}$H$_{22}$AuN$_4$O$_2$S$_{12}$	C$_{26}$H$_{22}$AuN$_4$O$_2$S$_{12}$
M [g mol^{-1}]	1004.16	1004.16	1004.16
T [K]	293(2)	293(2)	293(2)
crystal system	triclinic	triclinic	triclinic
space group	$P\bar{1}$	$P1$	$P1$
a [Å]	6.4501(6)	6.4515(9)	6.4531(3)
b [Å]	7.5111(5)	7.5392(9)	7.5337(4)
c [Å]	18.0943(15)	18.074(2)	18.0853(12)
α [°]	98.710(6)	98.116(14)	98.157(6)
β [°]	93.843(7)	93.877(16)	93.846(4)
γ [°]	94.255(6)	94.437(16)	94.477(5)
V [Å^3]	861.40(12)	864.96(19)	864.95(8)
Z	2	2	2
ρ_{calcd} [g cm^{-3}]	1.936	1.928	1.928
μ [mm^{-1}]	5.031	5.011	5.011
$F(000)$	493	493	493
GOF on F^2	1.019	0.885	1.017
final $R1$, wR^2 [$I > 2\sigma(I)$]	0.0626, 0.1330	0.0521, 0.1193	0.0428, 0.0926
$R1$, wR_2 (all data)	0.1467, 0.1561	0.0948, 0.1341	0.0784, 0.1041
largest diff. peak and hole [e Å^{-3}]	1.159, −1.155	0.957, −1.271	1.173, −0.958

two independent donor molecules together with the anion in general positions. The only small difference between the

crystal structure parameters of the two series of AsF_6^- and PF_6^- salts concerns the unit cell volume, which is on average about 7 Å^3 larger for the former than for the latter, a value that finds its origin in the larger size of the AsF_6^- anion compared with PF_6^-, in good agreement with other reported isostructural series.[23] Representative bond lengths for the oxidized donor in the three salts are listed in Table 2. It is known that the central C≡C bond lengthens upon oxidation, whereas the internal C−S bonds shorten, in agreement with the shape of the HOMO, which contains bonding and anti-bonding combinations, respectively (see also the Supporting Information).

In the racemic salt [(rac)-**1**]$_2$PF$_6$ the oxazoline ring is found to be disordered over two positions with a site occupational factor (s.o.f.) refined to 0.6 (R enantiomer, dark grey in Figure 3) and 0.4 (S enantiomer, light grey in Figure 3), in line with the earlier results for the [(rac)-**1**]$_2$AsF$_6$ salt,[19] for which the same type of disorder was observed.
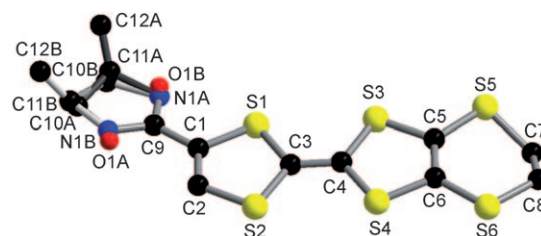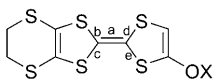

Figure 3. View of the donor molecule in [(rac)-**1**]$_2$PF$_6$ with an emphasis on the occupational disorder of the oxazoline ring (R enantiomer in dark grey at s.o.f. 0.6 and S enantiomer in light grey at s.o.f. 0.4). Hydrogen atoms have been omitted for clarity.

The oxazoline ring is practically coplanar with the TTF mean plane (see the Supporting Information), as ascertained by the small values of the dihedral angles TTF⋯OX$_A$ (5.4°) and TTF⋯OX$_B$ (12.4°), and thus both s-trans and s-cis conformations are present in the structure of the racemic salt, albeit disordered on the same crystallographic site. The solid-state structure analysis of the enantiopure salts [(R)-**1**]$_2$PF$_6$ and [(S)-**1**]$_2$PF$_6$ revealed the presence of two independent donor molecules in the unit cell, each corresponding to s-trans (OX$_1$) and s-cis (OX$_{1A}$) conformations, respectively (Figure 4 for the R salt).

However, unlike the racemic salt, no occupational disorder in either of the two donor molecules is observed in the enantiopure salts, as already noticed in the AsF$_6^-$ series. Once again, very small deviations from coplanarity between TTF and the oxazoline rings of 7.6° (TTF⋯OX$_1$) and 6.6° (TTF⋯OX$_{1A}$) are observed. These planar conformations clearly favor the establishment of intermolecular interactions between the partially oxidized donors in the organic slabs. Indeed, classic organic/inorganic segregation is observed with TTF-oxazolines alternating in a head-to-tail manner within stacks along the b axis, which are separated by layers of anions along the c axis (Figure 5).

Table 2. Selected bond lengths in the TTF moieties of the PF_6^- and $Au(CN)_2^-$ salts of **1** from X-ray diffraction data.

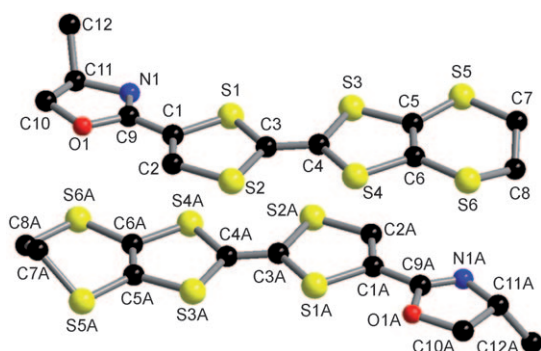|	Bond length [Å]					
	[(*rac*)-**1**]$_2$PF$_6$	[(*R*)-**1**]$_2$PF$_6$	[(*S*)-**1**]$_2$PF$_6$	[(*rac*)-**1**]$_2$[Au(CN)$_2$]	[(*R*)-**1**]$_2$[Au(CN)$_2$]	[(*S*)-**1**]$_2$[Au(CN)$_2$]
a	1.359(5)	1.383(7)	1.402(13)	1.375(9)	1.37(2)	1.342(11)
		1.353(7)	1.355(14)		1.36(2)	1.366(10)
b	1.738(3)	1.721(6)	1.717(10)	1.731(6)	1.733(13)	1.748(8)
		1.754(5)	1.747(10)		1.727(16)	1.728(8)
c	1.741(3)	1.740(6)	1.724(11)	1.740(6)	1.728(14)	1.732(8)
		1.730(7)	1.734(12)		1.751(17)	1.750(7)
d	1.744(3)	1.741(7)	1.729(12)	1.740(7)	1.762(15)	1.759(8)
		1.748(7)	1.739(12)		1.748(15)	1.749(8)
e	1.746(3)	1.745(6)	1.742(10)	1.743(6)	1.735(15)	1.740(8)
		1.739(6)	1.738(10)		1.731(14)	1.745(8)

Figure 4. View of the two independent donor molecules in [(*R*)-**1**]$_2$PF$_6$. Hydrogen atoms have been omitted for clarity.
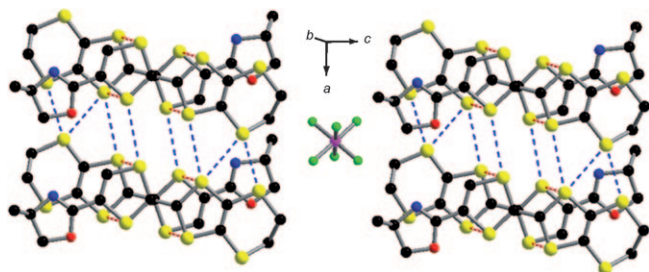

Figure 5. Projection view of the *ac* plane of the packing in [(*R*)-**1**]$_2$PF$_6$ with an emphasis on the organic/inorganic segregation; the short S···S contacts are highlighted in dotted red (intrastack) and blue (interstack) lines.
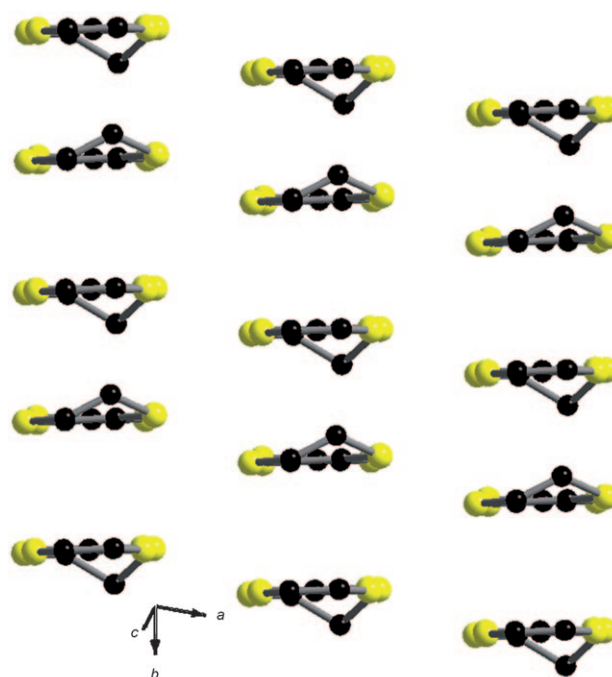

Figure 6. The β-type organic slab in [(*R*)-**1**]$_2$PF$_6$ viewed along the TTF core long axis. Oxazoline rings and hydrogen atoms have been omitted for clarity.

A set of several rather short interstack S···S contacts along the *a* axis, ranging between 3.28 and 3.43 Å, is observed, whereas the shortest intrastacking S···S distances along the *b* axis are 3.65–3.71 Å, at the limit of the van der Waals sum for two sulfur atoms (3.70 Å).[24] The parallel columns of donors give rise to organic slabs, which thus adopt a structural motif reminiscent of the β-type arrangement encountered in the BEDT-TTF-based salts (Figure 6).[25]

The opposite enantiomeric salt [(*S*)-**1**]$_2$PF$_6$, as well as the racemic one [(*rac*)-**1**]$_2$PF$_6$, present strictly the same packing features with similar values for the intermolecular S···S contacts (see the Supporting Information) and hence the intermolecular interaction energies are expected to be identical for the three compounds. This type of arrangement closely matches the one observed in the AsF$_6^-$ series.[19] Clearly the very fine tuning of the anion size on going from the AsF$_6^-$ to the PF$_6^-$ salts does not lead to a substantial change in the arrangements and disorder patterns of the donors in the solid state and therefore similar electronic properties are in principle expected (see below). This feature is not surprising because the isomorphous series of anions PF$_6^-$, AsF$_6^-$, and SbF$_6^-$ generally provide isostructural radical-cation TTF salts. Would the situation change with a different shaped monoanion?

Electrocrystallization of the same series of donors (*rac*)-, (*R*)-, and (*S*)-**1** in acetonitrile using this time the linear [Au(CN)$_2$]$^-$ anion as the tetrabutylammonium salt provided black needle-like crystals on the anode. Single-crystal X-ray diffraction study of the three salts shows a 2:1 donor-to-anion ratio and hence a mixed-valence state with a mean charge of $\delta = +0.5$ on each TTF. Once again, the cell parameters are identical for the whole series except for the space group, which is triclinic centrosymmetric $P\bar{1}$ for [(*rac*)-**1**]$_2$[Au(CN)$_2$] and triclinic noncentrosymmetric $P1$ for [(*R*)-**1**]$_2$[Au(CN)$_2$] and [(*S*)-**1**]$_2$[Au(CN)$_2$]. Moreover, only slight differences between the crystalline parameters of the two series of salts, that is, PF$_6^-$ and [Au(CN)$_2$]$^-$, can be observed (Table 1). Nevertheless, the independent donor molecule in the structure of [(*rac*)-**1**]$_2$[Au(CN)$_2$] crystallizes without any disorder of the oxazoline ring, unlike [(*rac*)-**1**]$_2$PF$_6$, as previously discussed. The two enantiomers are related through an inversion center and are present as the s-*trans* conformation (Figure 7).
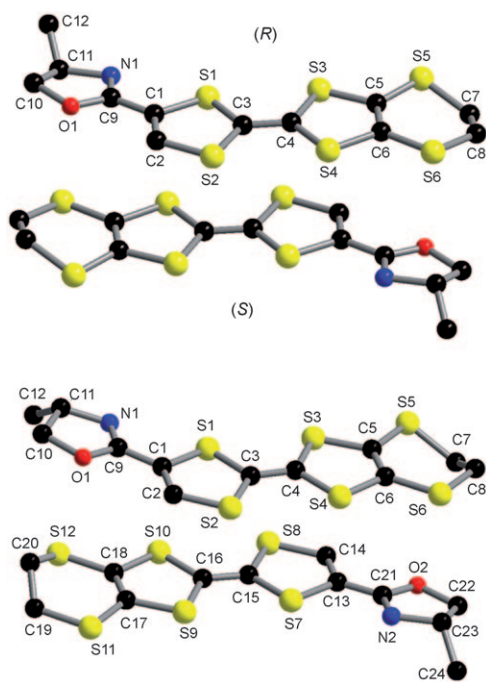

Figure 7. View of the centrosymmetric *R/S* dimer of donors in the structure of [(*rac*)-**1**]$_2$[Au(CN)$_2$] (top) and of the two independent donor molecules in the structure of [(*S*)-**1**]$_2$[Au(CN)$_2$] (bottom); only the s-*trans* conformation is observed. [Au(CN)$_2$]$^-$ anions and hydrogen atoms have been omitted for clarity.

The TTF···OX dihedral angle has a value of only 8.1°, which reveals the coplanarity between the two adjacent motifs. The enantiopure counterparts [(*R*)-**1**]$_2$[Au(CN)$_2$] and [(*S*)-**1**]$_2$[Au(CN)$_2$] crystallize with two independent donor molecules in the unit cell, yet, in contrast with the enantiopure salts with the PF$_6^-$ and AsF$_6^-$ anions, both are in the s-*trans* conformation (see Figure 7 and Supporting Information for the *S* and *R* enantiomers, respectively) with dihedral TTF···OX angles of 8.2–8.3°. As outlined above, the calcu-

lated energy difference between the two energy minima s-*cis* and s-*trans* is very small, and thus minute variations in the system, such as the shape of the anion, can promote the occurrence of only one or both of them in the solid state. The central C=C and C–S bonds are in the usual range for mixed-valence salts (Table 2). The packing pattern of the donors is identical for the three salts and consists of classic organic/inorganic segregation with slabs of organic donors organized in parallel columns as in the β-type phases (see Figure 8 for [(*rac*)-**1**]$_2$[Au(CN)$_2$] and the Supporting Information for the enantiopure salts).

The shortest interstack S···S distances are 3.33–3.76 Å along the *a* axis, whereas within the columns, S···S distances of 3.67 and 3.70 Å are observed between donors forming heterochiral centrosymmetric dimers for which the methyl substituents on the oxazoline rings point outwards (Figures 7
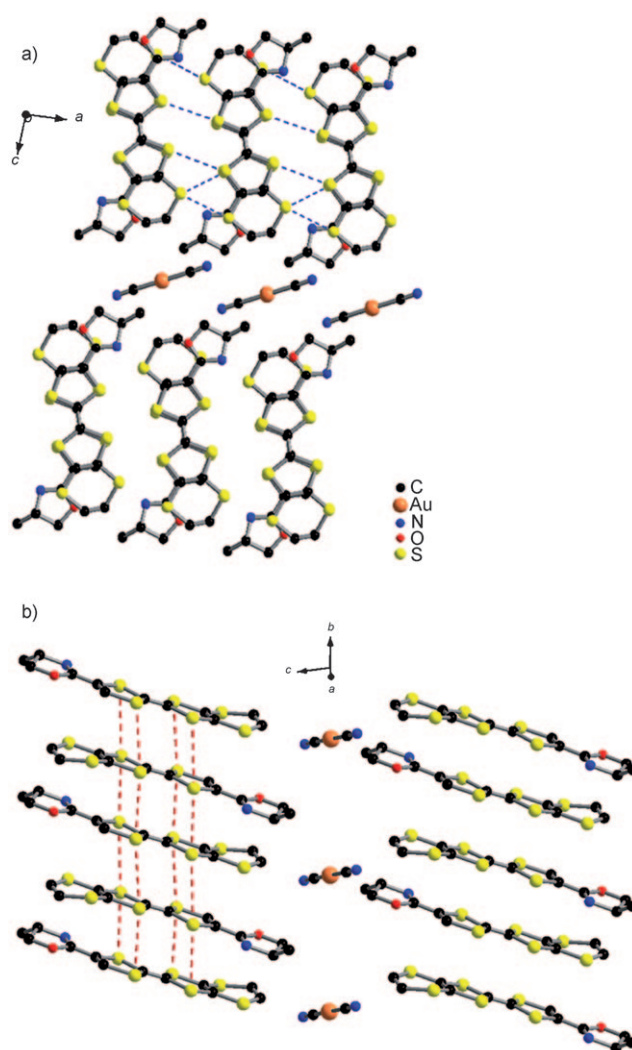

Figure 8. Projected view along the *ac* plane of the packing in [(*rac*)-**1**]$_2$[Au(CN)$_2$], with an emphasis on a) the organic/inorganic segregation and b) packing of the donors along the *b* axis. The short interstack (3.33–3.76 Å) and intrastack (3.67–3.84 Å) S···S contacts are highlighted by the blue and red dotted lines, respectively. Hydrogen atoms have been omitted for clarity.

and 8). On the other hand, the S⋯S distances are somewhat longer (3.82 and 3.84 Å) between donors with inward methyl substituents, which demonstrates that a certain degree of dimerization occurs in the chains. Although in the enantiopure salts the methyl substituents of the oxazoline rings are all oriented in the same direction, slight dimerization is also evident on the basis of the values of the intra-stack S⋯S distances (see the Supporting Information). The inorganic layer is formed by the linear $[Au(CN)_2]^-$ anions, with the metal lying on an inversion center. The shortest Au⋯Au distance is 6.45 Å along the *a* axis (Figure 8) and therefore no aurophilic interaction occurs.

From these results it is clear that from a structural point of view the strategy of influencing the order/disorder balance by introducing a small perturbation, that is, variation of the anion size and shape, in the chiral mixed-valence salt system appears to be particularly promising. In the first case the system preserves all the characteristics encountered in the series based on the AsF_6^- anion, whereas in the latter, suppression of the disorder on the oxazoline ring is observed together with the occurrence of only one out of the two stable conformations, that is, the s-*trans* conformation. Clearly, an important aspect concerns the effect of these structural features on the conducting properties of the two series of chiral salts.

Electronic conductivity properties and band structure calculations: As outlined in the Introduction, the three mixed-valence salts $[1]_2AsF_6$ previously described show metallic-like conductivity in the high-temperature regime with the room-temperature conductivity value being one order of magnitude higher for the enantiopure salts than for the racemic salt.[19] Indeed, the conductivity measured for a single crystal of the racemic salt is around 10 S cm^{-1}, whereas the conductivity for the enantiopure salts is an average of 100 S cm^{-1}. Needle-like single crystals of appropriate size for four-point resistivity measurements were obtained for the three salts of the $[1]_2PF_6$ series. For the racemic salt $[(rac)-1]_2PF_6$ a slight decrease in the resistivity is observed down to around 240 K, which indicates metallic behavior in this temperature range (Figure 9). Upon further cooling an activated regime is evident. Important to note is the room temperature conductivity of 5 S cm^{-1}, a value comparable to that obtained for the $[(rac)-1]_2AsF_6$ salt (see above).

The measurements performed in the case of the enantiopure salts $[(R)-1]_2PF_6$ and $[(S)-1]_2PF_6$ also demonstrate similar metallic-like behavior down to around 220 K followed by an activated regime characterized by a relatively weak activation energy of 17–25 meV (200–300 K; see Figure 10 and the Supporting Information for the S and R enantiomers, respectively). Interestingly, the average room-temperature conductivity is 110 S cm^{-1} with variations of ±25 S cm^{-1} depending on the quality of the crystal.

Thus, the conductivity properties we observe with the PF$_6^-$ series parallel to a great extent those described for the isostructural AsF$_6^-$ series, which is somehow expected when considering their similar packing in the solid state. Once
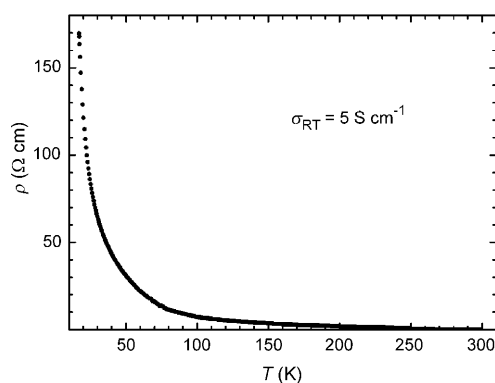

Figure 9. Temperature dependence of the electrical resistivity for a single crystal of $[(rac)-1]_2PF_6$.
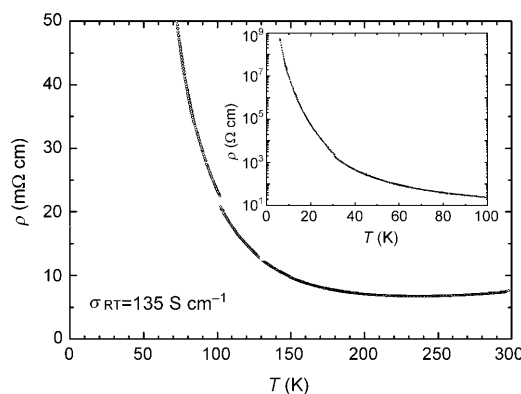

Figure 10. Temperature dependence of the electrical resistivity for a single crystal of $[(S)-1]_2PF_6$. The discontinuity in the curve is due to microcracks in the crystal occurring during the cooling process. Inset: low-temperature regime; note the log scale for resistivity.

again, the modulation of the solid-state structural disorder, which arises through the introduction of chiral information in the electroactive precursors, provokes a striking difference in the conductivity between the racemic and enantiopure forms, despite the closely related structures.

In the second series of mixed-valence salts, $[1]_2[Au(CN)_2]$, appropriately sized single crystals for conductivity measurements were obtained only for the racemic form and the R enantiomer. Metallic-like behavior is observed in the high-temperature regime, down to approximately 260 K, for $[(rac)-1]_2[Au(CN)_2]$ (Figure 11), yet the room-temperature conductivity is 125–130 S cm^{-1}, which is one order of magnitude higher than the value for $[(rac)-1]_2PF_6$.

Similarly, the conductivity measurements performed on $[(R)-1]_2[Au(CN)_2]$ also show metallic-like behavior down to 255 K, followed by an activated regime (Figure 12). Most important to note is the room-temperature conductivity of 125 S cm^{-1}, which is identical to that of the racemic salt.

Clearly these results emphasize and strengthen the conclusion we have previously reached, that the notable difference in conductivity observed between the racemic and enantiopure forms in the AsF$_6^-$ and PF$_6^-$ series is due to the
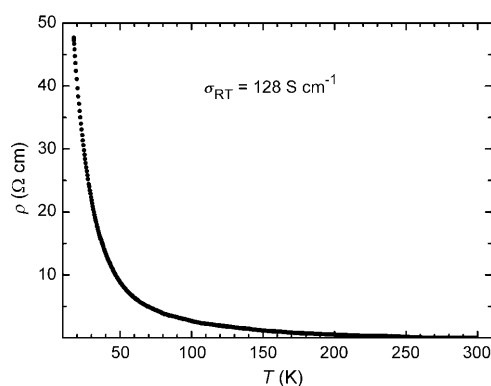
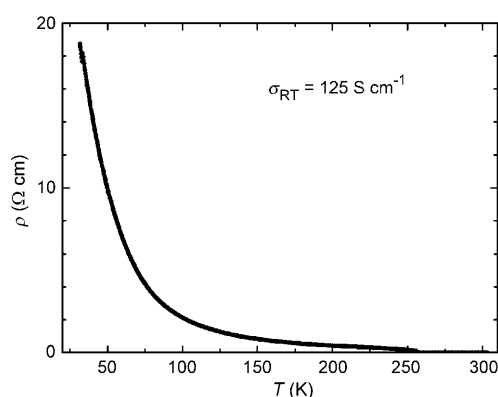Figure 11. Temperature dependence of the electrical resistivity for a single crystal of [(rac)-**1**]$_2$[Au(CN)$_2$].

Figure 12. Temperature dependence of the electrical resistivity for a single crystal of [(R)-**1**]$_2$[Au(CN)$_2$].

Figure 13. Slab of donors in the structure of [(rac)-**1**]$_2$[Au(CN)$_2$], with an emphasis on S···S intermolecular distances shorter than 4 Å, identified as interactions **I–IV**.

Table 3. Intermolecular interactions associated with S···S contacts shorter than 4 Å and with the corresponding interaction energies $|\beta_{HOMO–HOMO}|$ in [(rac)-**1**]$_2$[Au(CN)$_2$].

Interaction	S···S [Å]	$|\beta_{HOMO–HOMO}|$ [eV]
I	3.823 (×2), 3.844 (×2), 3.850 (×2), 3.948 (×2)	0.3349
II	3.671 (×2), 3.699 (×2)	0.5291
III	3.331, 3.404, 3.691, 3.760, 3.864	0.0561
IV	3.753 (×2), 3.975	0.1072

structural disorder in the donors mediated by the chirality of the oxazoline ring. Indeed, when no structural disorder occurs in either the racemic or enantiopure salts, as is the case with the [Au(CN)$_2$]$^-$ series, the same conductivity values are measured.

Band structure calculations for [**1**]$_2$AsF$_6$ were consistent with an open Fermi surface, typical of quasi-one-dimensional systems.[19] Much stronger intrastack than interstack contacts were observed, based on the intermolecular $\beta_{HOMO–HOMO}$ interaction energies,[26] calculated by the extended Hückel method. Evidently, these features are the same for the isostructural [**1**]$_2$PF$_6$ series. We have therefore performed $\beta_{HOMO–HOMO}$ interaction energies and tight-binding calculations only for the [**1**]$_2$[Au(CN)$_2$] salts. Because they present identical structural features, the results are, as anticipated, the same for the three compounds. Four different interactions, that is, two intrastack (**I** and **II**) and two interstack (**III** and **IV**), have been identified in the β-type organic slab of [(rac)-**1**]$_2$[Au(CN)$_2$] (Figure 13), for which $\beta_{HOMO–HOMO}$ interaction energies have been determined (Table 3).

Thus, it appears that the intrastack interactions **I** (0.3349 eV) and **II** (0.5291 eV) are much stronger than the interstack interactions **III** (0.0561 eV) and **IV** (0.1072 eV),
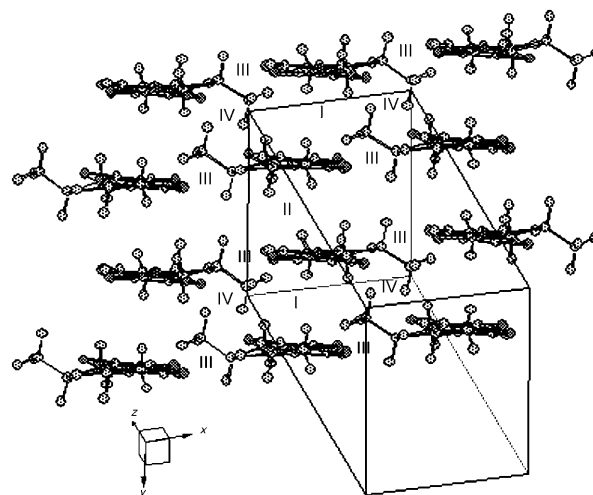
which is to be compared with a typical β phase like β-(BEDT-TTF)$_2$I$_3$[26] for which the energy difference between the two sets of interactions is smaller. As a consequence, the Fermi level in the latter cuts the energy bands in both directions thus providing a closed Fermi surface, whereas in the former, only the Γ–Y band, which corresponds to the intrastack interactions along the b axis, is intersected by the Fermi level (Figure 14). Therefore, in this case, the Fermi surface consists of a pair of warped lines characterizing a quasi-one-dimensional system (Q1D), as also observed with the AsF$_6$$^-$ series.

Identical features were determined for the [(R)-**1**]$_2$[Au(CN)$_2$] and [(S)-**1**]$_2$[Au(CN)$_2$] salts (see the Supporting Information). When considering the smoothness of the resistivity increase (Figures 11 and 12) at lower temperatures, it appears more likely that the semiconducting regime is a consequence of a 1D Mott localization of the charge carriers[27] rather than a charge density wave (CDW) transition. The overall conducting behavior of the [**1**]$_2$[Au(CN)$_2$] salts, as well as the electronic structure estimated through band structure calculations, strongly resemble those of the [**1**]$_2$AsF$_6$ series. Nevertheless, as already pointed out, the only striking difference is related to the remarkably low value of the conductivity of the racemic salts with AsF$_6$$^-$ and PF$_6$$^-$ anions compared with their enantiopure counter-
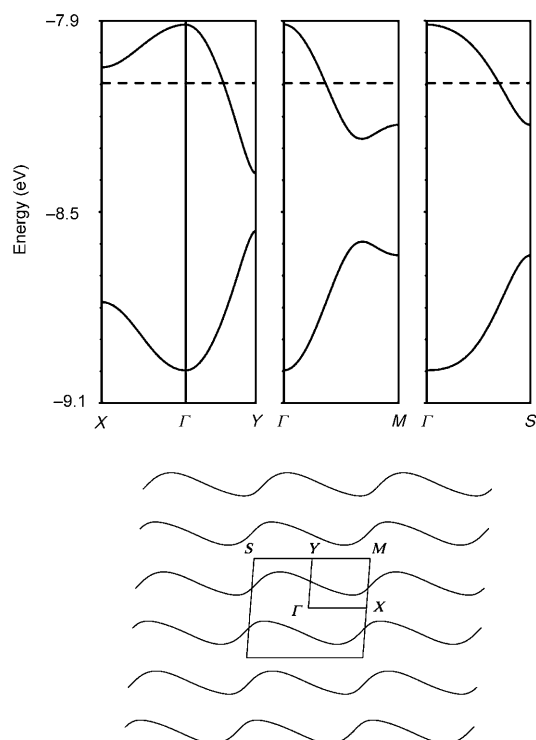
Figure 14. Calculated band structure for $[(rac)\text{-}\mathbf{1}]_2[Au(CN)_2]$ (top) and calculated Fermi surface for the donor layers (bottom). $\Gamma = (0, 0)$, $X = (a^*/2, 0)$, $Y = (0, b^*/2)$, $M = (a^*/2, b^*/2)$ and $S = (-a^*/2, b^*/2)$.

parts as well as the $[Au(CN)_2]^-$ series, a likely consequence of the interplay between chirality and structural disorder.

Conclusion

Two new complete series of crystalline mixed-valence radical-cation salts based on chiral EDT-TTF-methyl-oxazoline (EDT-TTF-OX) donors and PF_6^- and $[Au(CN)_2]^-$ anions have been obtained by electrocrystallization and characterized by single-crystal X-ray analyses. The former series was found to be isostructural with members of the previously described AsF_6^- counterpart, showing the occurrence of both s-cis and s-trans conformations of the donors in the oxidized state. The relative energy of the two planar stable conformations was estimated for a simple TTF-oxazoline by DFT calculations. A very weak energy difference between the s-cis and s-trans conformations, with a slightly more stable geometry for the latter, was found both in the neutral and oxidized states, which allows us to conclude that the occurrence in the solid state of either one or other conformation can be influenced by subtle variations in the intermolecular interactions and/or packing effects. Thus, the slight decrease in the anion size from AsF_6^- to PF_6^- provided the same solid-state patterns, the main one being the disorder observed in the racemic form, with both enantiomers present on the same crystallographic sites. In contrast, with the $[Au(CN)_2]^-$

anion, no structural disorder was observed in either the racemic or enantiopure compounds.

The electronic conductivity of these new chiral molecular conductors was measured on single crystals with metallic behavior observed in the high-temperature regime. Most interestingly, the conductivity of the disordered racemic form of the PF_6^- series is one order of magnitude lower than that of the corresponding enantiopure forms, for which the room-temperature conductivity is roughly the same value as for the $[Au(CN)_2]^-$ series, with no disorder at all. According to the band structure calculations these are quasi-one-dimensional conductors, despite the β-type arrangement of the donors. These results highlight one of the possible roles of chiral information in the field of molecular materials, the modulation of structural disorder, and emphasize the diversity and versatility of the TTF-oxazoline class of donors in the preparation of chiral conductors.

Experimental Section

Electrocrystallization: Donor **1** was prepared according to the published procedure.[11] A two-compartment cell was used together with platinum electrodes (2 cm long, 1 mm in diameter) and a current of 1 μA at room temperature $(20 \pm 2\,^\circ\mathrm{C})$. $[(nBu)_4N]PF_6$ (100 mg) or $[(nBu)_4N][Au(CN)_2]$ (60 mg) in CH_3CN (14 mL) were used as the electrolyte, with the donor **1** (5–7 mg) dissolved in the anodic compartment. Electrolysis was performed over 7 days after which air-stable black-brown needle-like crystals were harvested on the anode.

X-ray structure determinations: Details of data collection and solution refinement are given in Table 1. X-ray diffraction measurements were performed on a Bruker Kappa CCD diffractometer for $[(R)\text{-}\mathbf{1}]_2PF_6$, $[(rac)\text{-}\mathbf{1}]_2[Au(CN)_2]$, and $[(S)\text{-}\mathbf{1}]_2[Au(CN)_2]$ and on a Stoe Imaging Plate System for $[(rac)\text{-}\mathbf{1}]_2PF_6$, $[(S)\text{-}\mathbf{1}]_2PF_6$, and $[(R)\text{-}\mathbf{1}]_2[Au(CN)_2]$, both operating with a $Mo_{K\alpha}$ ($\lambda = 0.71073$ Å) X-ray tube with a graphite monochromator. The structures were solved (SHELXS-97) by direct methods and refined (SHELXL-97) by full-matrix least-squares procedures on F^2.[28] All non-hydrogen atoms were refined anisotropically whereas hydrogen atoms were introduced at calculated positions (riding model), included in structure factor calculations, but not refined.

CCDC-739465 ($[(rac)\text{-}\mathbf{1}]_2PF_6$), 739466 ($[(R)\text{-}\mathbf{1}]_2PF_6$), 739467 ($[(S)\text{-}\mathbf{1}]_2PF_6$), 739468 ($[(rac)\text{-}\mathbf{1}]_2[Au(CN)_2]$), 739469 ($[(R)\text{-}\mathbf{1}]_2[Au(CN)_2]$), and 739470 ($[(S)\text{-}\mathbf{1}]_2[Au(CN)_2]$) contain the supplementary crystallographic data for this paper. These data can be obtained free of charge from The Cambridge Crystallographic Data Centre via www.ccdc.cam.ac.uk/data_request/cif.

Theoretical calculations: The optimized geometries were obtained with the Gaussian 03[29] package at the DFT level of theory. The B3LYP functional[30] with the 6-31+G* basis set was used. Vibration frequency calculations performed on the optimized structures at the same level of theory yielded only positive values. The input geometries for s-trans $\mathbf{1}'$, s-trans $[\mathbf{1}']^{+\bullet}$, and s-cis $[\mathbf{1}']^{+\bullet}$ were constructed starting from the experimental X-ray structures of **1** and $[\mathbf{1}]^{+\bullet}$, whereas that for s-cis $\mathbf{1}'$ was obtained by rotating the oxazoline ring of s-trans $\mathbf{1}'$ by 180°. The tight-binding band structure calculations were of the extended Hückel type[31a] performed with a modified Wolfsberg–Helmholtz formula to calculate the nondiagonal $H_{\mu\nu}$ values.[31b] The basis set consisted of double-ζ Slater-type orbitals for carbon, nitrogen, oxygen, and sulfur atoms and single-ζ Slater-type orbitals for hydrogen atoms. The exponents, contraction coefficients, and ionization potentials were taken from previous work.[32]

Single-crystal conductivity measurements: Electrical resistivity was measured on needle-like crystals. Indexation of the crystal faces of several crystals exhibiting the same shape proved that the long axis of the crystal is indeed the stacking b axis. Four gold contacts were evaporated along

the long axis of the crystals and all around it and gold wires were glued with silver paste to those contacts. Resistivity measurements were performed in the range 4–300 K using a four-point method. A low frequency (<100 Hz) lock-in technique with a measuring current $I_{ac} = 1$ μA was used for resistance values of less than 50 kOhm, whereas higher resistances were measured with dc currents ranging from 100 to 0.5 nA.

Acknowledgements

[1] a) E. Coronado, P. Day, *Chem. Rev.* **2004**, *104*, 5419–5448; b) E. Coronado, J. R. Galán-Mascarós, *J. Mater. Chem.* **2005**, *15*, 66–74.

[2] N. Avarvari, J. D. Wallis, *J. Mater. Chem.* **2009**, *19*, 4061–4076.

[3] G. L. J. A. Rikken, J. Folling, P. Wyder, *Phys. Rev. Lett.* **2001**, *87*, 236602–236601-4.

[4] a) V. Krstić, S. Roth, M. Burghard, K. Kern, G. L. J. A. Rikken, *J. Chem. Phys.* **2002**, *117*, 11315–11319; b) V. Krstić, G. L. J. A. Rikken, *Chem. Phys. Lett.* **2002**, *364*, 51–56.

[5] a) G.-L. Yuan, N. Kuramoto, *Macromolecules* **2003**, *36*, 7939–7945; b) D. Cornelis, H. Peeters, S. Zrig, B. Andrioletti, E. Rose, T. Verbiest, G. Koeckelberghs, *Chem. Mater.* **2008**, *20*, 2133–2143.

[6] E. Gomar-Nadal, J. Veciana, C. Rovira, D. B. Amabilino, *Adv. Mater.* **2005**, *17*, 2095–2098.

[7] T. Yamamoto, T. Fukushima, A. Kosaka, W. Jin, Y. Yamamoto, N. Ishii, T. Aida, *Angew. Chem.* **2008**, *120*, 1696–1699; *Angew. Chem. Int. Ed.* **2008**, *47*, 1672–1675.

[8] a) J. M. Williams, J. R. Ferraro, R. J. Thorn, K. D. Carlson, U. Geiser, H. H. Wang, A. M. Kini, M.-H. Whangbo, *Organic Superconductors (Including Fullerenes), Synthesis Structure, Properties and Theory* (Ed.: R. N. Grimes), Prentice-Hall, Englewoods, **1992**; b) T. Ishiguro, K. Yamaji, G. Saito, *Organic Superconductors*, Springer, Heidelberg, **1998**.

[9] a) J. L. Segura, N. Martin, *Angew. Chem.* **2001**, *113*, 1416–1455; *Angew. Chem. Int. Ed.* **2001**, *40*, 1372–1409; b) J.-L. Yamada, *TTF Chemistry: Fundamentals and Applications of Tetrathiafulvalene*, Springer, Berlin, **2004**; c) D. Lorcy, N. Bellec, M. Fourmigué, N. Avarvari, *Coord. Chem. Rev.* **2009**, *253*, 1398–1438; d) D. Canevet, M. Sallé, G. Zhang, D. Zhang, D. Zhu, *Chem. Commun.* **2009**, 2245–2269.

[10] a) J. D. Wallis, J.-P. Griffiths, *J. Mater. Chem.* **2005**, *15*, 347–365; b) J.-P. Griffiths, N. Hui, R. J. Brown, P. Day, J. D. Wallis, *Org. Biomol. Chem.* **2005**, *3*, 2155–3379.

[11] a) C. Réthoré, M. Fourmigué, N. Avarvari, *Chem. Commun.* **2004**, 1384–1385; b) C. Réthoré, M. Fourmigué, N. Avarvari, *Tetrahedron* **2005**, *61*, 10935–10942.

[12] F. Riobé, N. Avarvari, *Chem. Commun.* **2009**, 3753–3755.

[13] E. Gomar-Nadal, C. Rovira, D. B. Amabilino, *Tetrahedron* **2006**, *62*, 3370–3379.

[14] S. Yang, A. C Brooks, L. Martin, P. Day, H. Li, P. Horton, L. Male, J. D. Wallis, *CrystEngComm* **2009**, 11, 993–996.

[15] a) M. Chas, M. Lemarié, M. Gulea, N. Avarvari, *Chem. Commun.* **2008**, 220–222; b) M. Chas, F. Riobé, R. Sancho, C. Minguíllon, N. Avarvari, *Chirality* **2009**, *21*, 818–825.

[16] J. D. Dunitz, A. Karrer, J. D. Wallis, *Helv. Chim. Acta* **1986**, *69*, 69–70.

[17] A. Karrer, J. D. Wallis, J. D. Dunitz, B. Hilti, C. W. Mayer, M. Bürkle, J. Pfeiffer, *Helv. Chim. Acta* **1987**, *70*, 942–953.

[18] J. S. Zambounis, C. W. Mayer, K. Hauenstein, B. Hilti, W. Hofherr, J. Pfeiffer, M. Buerkle, G. Rihs, *Adv. Mater.* **1992**, *4*, 33–35.

[19] C. Réthoré, N. Avarvari, E. Canadell, P. Auban-Senzier, M. Fourmigué, *J. Am. Chem. Soc.* **2005**, *127*, 5748–5749.

[20] a) G. Grüner, *Rev. Mod. Phys.* **1988**, *60*, 1129–1181; b) D. Jérome, H. J. Schulz, *Adv. Phys.* **1982**, *31*, 299–490.

[21] L. Martin, P. Day, H. Akutsu, J. Yamada, S. Nakatsuji, W. Clegg, R. W. Harrington, P. N. Horton, M. B. Hursthouse, P. McMillan, S. Firth, *CrystEngComm* **2007**, *9*, 865–867.

[22] C. Réthoré, A. Madalan, M. Fourmigué, E. Canadell, E. B. Lopes, M. Almeida, R. Clérac, N. Avarvari, *New J. Chem.* **2007**, *31*, 1468–1483.

[23] R. Clérac, M. Fourmigué, J. Gaultier, Y. Barrans, P. A. Albouy, C. Coulon, *Eur. Phys. J. B* **1999**, *9*, 431–443.

[24] a) A. Bondi, *J. Phys. Chem.* **1964**, *68*, 441–451; b) M. A. Spackman, *J. Chem. Phys.* **1986**, *85*, 6579–6586.

[25] T. Mori, *Bull. Chem. Soc. Jpn.* **1998**, *71*, 2509–2526.

[26] M.-H. Whangbo, J. M. Williams, P. C. W. Leung, M. A. Beno, T. J. Emge, H. H. Wang, *Inorg. Chem.* **1985**, *24*, 3500–3502.

[27] D. Jérome, *Chem. Rev.* **2004**, *104*, 5565–5591.

[28] G. M. Sheldrick, SHELXL91, Release 97-2, Program for the Refinement of Crystal Structures, University of Göttingen, Göttingen (Germany), **1997**.

[29] Gaussian 03, Revision B.03, M. J. Frisch, G. W. Trucks, H. B. Schlegel, G. E. Scuseria, M. A. Robb, J. R. Cheeseman, J. A. Montgomery, Jr., T. Vreven, K. N. Kudin, J. C. Burant, J. M. Millam, S. S. Iyengar, J. Tomasi, V. Barone, B. Mennucci, M. Cossi, G. Scalmani, N. Rega, G. A. Petersson, H. Nakatsuji, M. Hada, M. Ehara, K. Toyota, R. Fukuda, J. Hasegawa, M. Ishida, T. Nakajima, Y. Honda, O. Kitao, H. Nakai, M. Klene, X. Li, J. E. Knox, H. P. Hratchian, J. B. Cross, V. Bakken, C. Adamo, J. Jaramillo, R. Gomperts, R. E. Stratmann, O. Yazyev, A. J. Austin, R. Cammi, C. Pomelli, J. W. Ochterski, P. Y. Ayala, K. Morokuma, G. A. Voth, P. Salvador, J. J. Dannenberg, V. G. Zakrzewski, S. Dapprich, A. D. Daniels, M. C. Strain, O. Farkas, D. K. Malick, A. D. Rabuck, K. Raghavachari, J. B. Foresman, J. V. Ortiz, Q. Cui, A. G. Baboul, S. Clifford, J. Cioslowski, B. B. Stefanov, G. Liu, A. Liashenko, P. Piskorz, I. Komaromi, R. L. Martin, D. J. Fox, T. Keith, M. A. Al-Laham, C. Y. Peng, A. Nanayakkara, M. Challacombe, P. M. W. Gill, B. Johnson, W. Chen, M. W. Wong, C. Gonzalez, J. A. Pople, Gaussian, Inc., Wallingford CT, **2004**.

[30] a) C. Lee, W. Yang, R. G. Parr, *Phys. Rev. B* **1988**, *37*, 785–789; b) A. D. Becke, *J. Chem. Phys.* **1993**, *98*, 5648–5652.

[31] a) M.-H. Whangbo, R. Hoffmann, *J. Am. Chem. Soc.* **1978**, *100*, 6093–6098; b) J. H. Ammeter, H.-B. Bürgi, J. Thibeault, R. Hoffmann, *J. Am. Chem. Soc.* **1978**, *100*, 3686–3692.

[32] a) A. Pénicaud, K. Boubekeur, P. Batail, E. Canadell, P. Auban-Senzier, D. Jérome, *J. Am. Chem. Soc.* **1993**, *115*, 4101–4112; b) S. A. Baudron, N. Avarvari, E. Canadell, P. Auban-Senzier, P. Batail, *Chem. Eur. J.* **2004**, *10*, 4498–4511.